Budgeted Broadcast: An Activity-Dependent Pruning Rule for Neural Network Efficiency

Yaron Meirovitch^{1,*,†} Fuming Yang^{1,*,†} Jeff W. Lichtman^{1,†} Nir Shavit^{2,3,†}

¹Harvard University ²MIT ³Red Hat AI

Abstract

Most pruning methods remove parameters ranked by impact on loss (e.g., magnitude or gradient). We propose Budgeted Broadcast (BB), which gives each unit a local traffic budget—the product of its long-term on-rate a_i and fan-out k_i . A constrained-entropy analysis shows that maximizing coding entropy under a global traffic budget yields a selectivity—audience balance, $\log \frac{1-a_i}{a_i} = \beta k_i$. BB enforces this balance with simple local actuators that prune either fan-in (to lower activity) or fan-out (to reduce broadcast). In practice, BB increases coding entropy and decorrelation and improves accuracy at matched sparsity across Transformers for ASR, ResNets for face identification, and 3D U-Nets for synapse prediction, sometimes exceeding dense baselines. On electron microscopy images, it attains state-of-the-art F1 and PR-AUC under our evaluation protocol. BB is easy to integrate and suggests a path towards learning more diverse and efficient representations.

1 Introduction

Biological neural circuits are masterpieces of efficiency, sculpted by evolution to operate under strict metabolic and material constraints. This constant pressure for resource optimization fosters diverse and robust neural codes capable of navigating a complex world. In stark contrast, modern deep neural networks, trained with abundant compute, often learn highly redundant representations and falter on rare, long-tail events. This gap raises a central question: can we instill a formal principle of biological resource efficiency into artificial neural networks to make them more robust and diverse?

To date, the vast literature on network pruning has focused almost exclusively on a neuron's *utility*: its importance as measured by weight magnitude, gradient information, or contribution to the loss. We argue that this network-level mechanism is overly opportunistic. Inspired by formal models of metabolic constraints in neuroscience [1], we introduce the orthogonal axis of a neuron's *cost*: the resources it consumes to broadcast its signal.

We formalize this cost as a neuron's traffic, $t_i = a_i k_i$: the product of how often it 'speaks' (its long-term firing rate, a_i) and the size of its 'audience' (its axonal fan-out, k_i). Our method, **Budgeted Broadcast (BB)**, directly enforces a local budget on this traffic. In its simplest form, a unit prunes its weakest connections if and only if its traffic t_i exceeds a threshold τ . Intuitively, this has a direct consequence of protecting highly selective, rare-feature detectors (low a_i) by treating them as metabolically cheap, while curtailing the fan-out of over-active, low-selectivity units. This enforces a tradeoff: neurons can 'speak' loudly to a small audience (high activity, low fan-out) or quietly to a large one (low activity, high fan-out), but not both. In contrast to "lazy-neuron" pruning (e.g., [2]), BB reallocates connectivity toward a more efficient and diverse code.

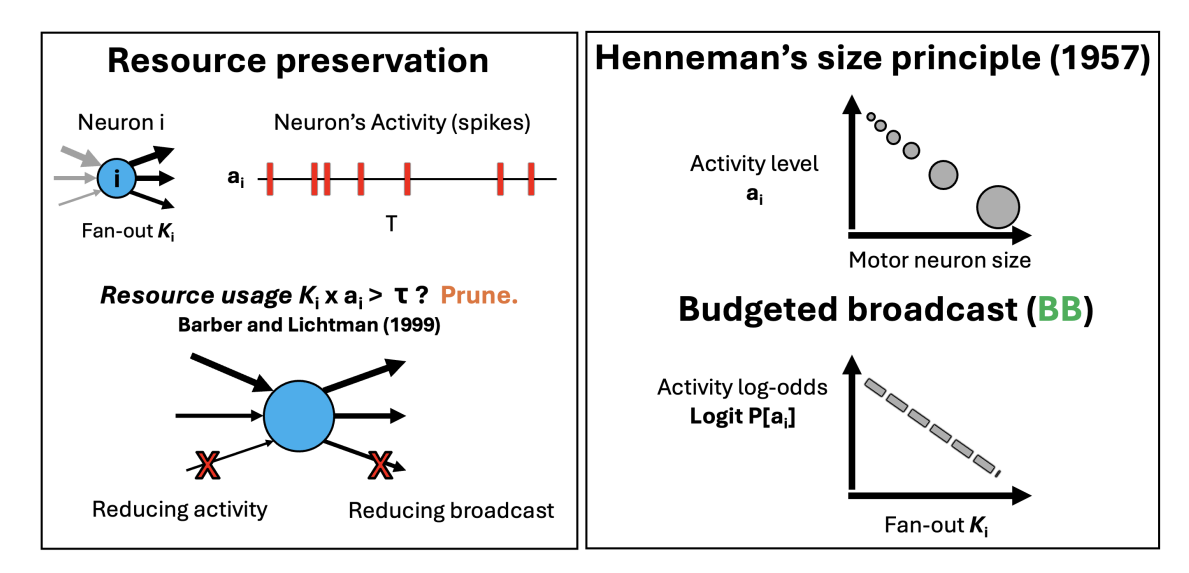


Figure 1: The conceptual framework of Budgeted Broadcast, from biology to a predictive theory. (Left) Our method models a neuron's metabolic cost as traffic, $t_i = a_i k_i$ (long-term activity × fan-out). If traffic exceeds a budget τ , connections are pruned. This can be achieved by reducing fan-out (axonal pruning) or reducing fan-in to lower activity (dendritic pruning). (**Top Right**) This rule is inspired by Henneman's size principle [4, 5], where large motor neurons (large size, analogous to fan-out k_i) have lower average activity levels (a_i). (**Bottom Right**) Our resource-preservation rule predicts a linear relationship between a unit's fan-out (k_i) and its inactivity log-odds ($\log \frac{a_i}{1-a_i}$), which we term the selectivity-audience balance.

This simple, local rule gives rise to a global organizing principle. An analysis of the network's coding entropy, which we detail later, predicts that this budget pressure drives the network to self-organize into a measurable equilibrium which we term *selectivity-audience balance* (Fig. 1, bottom right). In learned codes where unit activities are only weakly correlated [3], this balance is attained when the unit's fan-out k_i is proportional to its inactivity log-odds:

$$\log \frac{1 - a_i}{a_i} \approx \beta \, k_i.$$

This condition associates a unit's structure (node degree) to its function (node activity). We show that while it emerges as a regularity in a budgeted network, it is absent in networks trained (and/or pruned) with standard methods. In practice, we directly use this linear relationship to progressively modify the connections during learning.

Contributions. Our contributions follow a progression from empirical neuroscience to learning theory and ends with practical AI algorithms. First, we formalize a traffic budget, originally studied in the context of the neuromuscular connectome, via a constrained-entropy objective, deriving a testable *selectivity-audience* balance ($\log \frac{1-a_i}{a_i} = \beta k_i$) as the system's equilibrium state. We then implement this as a minimal, local controller, BB. We validate its properties on controlled didactic tasks, showing that it (1) verifiably produces the predicted balance, (2) provides structural safety for rare-but-relevant signals, and (3) overcomes optimization barriers that stall standard gradient-based methods. Finally, we demonstrate the utility of a general form of BB across four domains: ASR, face identification, synapse detection, and change detection, where it consistently improves tail/rare-event metrics at matched sparsity (Sec. 5.2, 5.3, 5.4, 5.5).

2 Related Work

Many pruning algorithms have been studied in the past decade. Magnitude pruning removes small weights and has underpinned compression work (6, 7); MorphNet uses layer-wise L_1 costs (8); Hessian and early saliency methods optimize local criteria (9); the Lottery Ticket line studies sparse trainable subnets [10]; and SynFlow prunes using a connectivity-sensitivity proxy [11]. Closest to our model is the bipartite-matching model of Dasgupta et al. [12], which simulates neural competition and reallocation of resources across outgoing edges.

Like Dasgupta et al., our approach draws inspiration from biological principles but differs fundamentally from existing pruning methods in both motivation and mechanism.

Activity-dependent synapse elimination: Our work operationalizes a specific form of homeostatic regulation observed during neural development: activity-dependent synapse elimination. This process is captured by the two-force dynamic model of the neuromuscular junction of Barber and Lichtman [1], in which a neuron's finite metabolic budget induces a trade-off between firing rate and audience size—high a_i to few targets (low k_i) or low a_i to many (high k_i). Our traffic metric $t_i = a_i k_i$ is the direct computational expression of this trade-off. We translate the model's forces into our rule: (1) the presynaptic resource limit becomes the budget gate $t_i > \tau$ that triggers pruning, and (2) postsynaptic competition is modeled by removing the weakest outgoing weight $|w_{ij}|$. BB therefore implements structural homeostasis, turning foundational neurodevelopmental principles into a practical algorithm for sculpting network connectivity.

Activity-Based Pruning: Methods that prune based on activity (a_i) alone are an intuitive starting point, but they risk conflating a neuron's importance with its firing rate. In contrast, BB's traffic metric $t_i = a_i k_i$ is more nuanced in intuiting that a highly selective unit (low a_i) may be critically important and thus require a large audience (high k_i), hence protecting this 'quiet specialist.'

Gradient-Based Methods: SNIP and GraSP estimate importance from gradients [14, 15], while methods like RigL use gradient information to guide dynamic regrowth. While effective, these approaches rely on optimization signals that may lag optimal connectivity patterns. Unlike these gradient-driven methods, BB is a developmental controller derived from first principles. It operates using local, label-free statistics (a_i, k_i) and can reshape connectivity independently of gradient updates, acting as an autonomous homeostatic process analogous to biological circuit refinement.

Structured Patterns: While hardware-aligned patterns like N:M sparsity deliver predictable speedups, our focus is on the *allocation principle* rather than the implementation pattern. BB can first allocate audience under a budget, then the resulting connectivity can be projected to hardware-friendly patterns for deployment-separating the biological principle from engineering constraints.

3 Method — Budgeted Broadcast (Local Broadcast Rule)

Our method, Budgeted Broadcast (BB), is governed by a local traffic-control rule. For each unit i, we periodically evaluate its traffic score:

$$t_i = a_i \cdot k_i$$

where a_i is the long-term average activation (on-rate), tracked via an Exponential Moving Average (EMA), and k_i is its current fan-out. If t_i exceeds a predefined budget τ , the unit is marked for pruning in either or both ways: 1) A fraction of its weakest outgoing connections is removed (an 'SP-out' action), directly reducing k_i to bring the unit back within budget. 2) incoming connections are removed (an 'SP-in' action) to reduce the neuron's activity a_i . These actions force a reallocation of network connectivity from high-traffic to low-traffic units. In practice, we keep each unit's "audience" proportional to how quiet or busy it is. Let \tilde{a} be a unit's activity Exponential Moving Average (EMA); the target degree is

$$k = d_0 + \beta^{-1} \log \frac{1 - \tilde{a}}{\tilde{a}}, \quad k \in [m, D].$$

SP-out (activation-aware fan-out pruning)

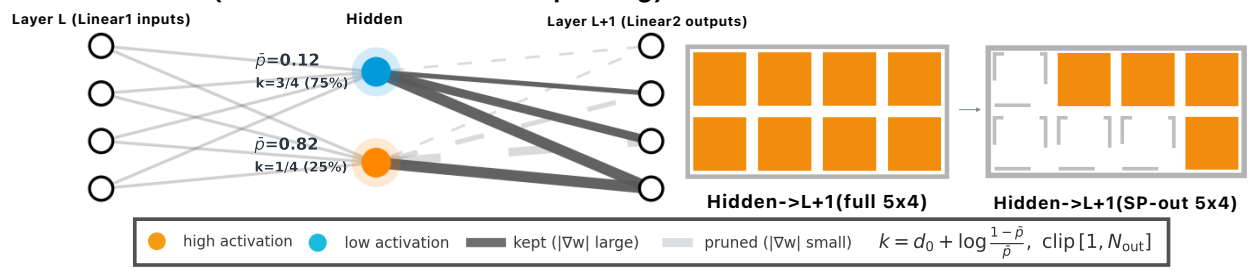


Figure 2: **SP-out** (**Axonal pruning**). Activation-aware fan-out pruning that masks a hidden unit's outgoing connections to the next layer, enforcing the per-unit traffic budget t = a k against a metabolic threshold τ . High-activity units (large a) shed more outgoing edges; low-activity units keep more. Right: the learned binary mask sparsifies the dense hidden $\to L+1$ matrix according to $k = d_0 + \frac{1}{\beta} \log \frac{1-a}{a}$, clipped to $[1, N_{\text{out}}]$. **SP-in** performs the complementary, opposite operation (fan-in pruning); see Appendix.

Every Δ step we recompute k per unit and reselect Top-k by |W|, enabling natural regrowth. We apply this at FFN fan-in (SP-in) and optionally fan-out (SP-out), with a variance-preserving rescale to keep layer scale stable.

Entropy maximization. This degree controller satisfies the conditions needed to globally maximize coding entropy H(h) of the network, subject to a total traffic budget $\sum_i a_i k_i \leq T_{\text{max}}$. The Lagrangian $\mathcal{L} = H(h) - \beta \left(\sum_i a_i k_i - T_{\text{max}} \right)$ is stationary for $\log \frac{1-a_i}{a_i} = \beta k_i$ consistently with the controller (see Appendix for the full derivation).

In practice, we implement BB inside FFN blocks (the 1×1 paths) by multiplying W_1 and W_2 with binary masks that refresh periodically (Fig. 2). For simplicity, most of our theory is derived for the SP-out actuators: at the first projection W_1 , row masks (SP-out@ W_1) limit a source unit's broadcast by reducing its fan-out k; at the second projection W_2 , row masks (SP-out@ W_2) analogously limit a hidden unit's broadcast. We provide in the appendix theoretical accounts for the complementary SP-in actuator, implemented as column masks at W_1 that reduce fan-in to modulate activity a (Appendix). In this work, other components (e.g., attention, embeddings) remain dense. To minimize overhead, we avoid per-weight counters and store only a channel-wise EMA and the binary masks. While our method induces unstructured sparsity, mapping the learned masks to structured patterns (e.g., N:M sparsity) is a deployment step deferred to future research.

4 Theory

A central question is why a simple, local pruning rule should lead to a globally coherent and efficient network structure. We get some insight by viewing our rule as a decentralized algorithm for solving a global optimization problem. Imagine we could design the network's connectivity to perfectly adhere to its function (a 'god's-eye view') with the goal of maximizing the total information-coding capacity of the hidden units (measured by their entropy), subject to a fixed total 'energy' budget.

While this constrained-entropy view implicitly leads to the selectivity-audience balance $\log \frac{1-a_i}{a_i} = \beta k_i$ (formally derived in the appendix), we can establish a more direct link between our local rule and the network's function using information theory. Under a standard noisy channel model for interlayer communication (see Assumption A1 in Appendix) the mutual information I(Z;Y) between a layer's code Z and the next layer's preactivations Y is upper-bounded by the trace of the output covariance: $I(Z;Y) \leq \frac{1}{2\sigma^2} \operatorname{tr}(W^{\mathsf{T}} \operatorname{Cov}(Z)W)$. When correlations are weak (a regime BB and SGD promote and we observe empirically) and weights are

Algorithm 1: Budgeted Broadcast (SP-in/SP-out Refresh)

```
Input: W \in \mathbb{R}^{R \times C}; mask M; activity EMA a_{\text{ema}}
   Output: updated mask M
   Parameters: schedule params: step, T_{\text{warmup}}, \Delta; rule params: \alpha, \beta, d_0; bounds m, D; flag SP_IN
 2 if step < T_{warmup} or step \mod \Delta \neq 0 then
        return M
 4 for u \leftarrow 1 to U do
        k \leftarrow \text{clip}() \left(d_0 + \beta^{-1} \log \frac{1 - a_{\text{ema}}[u]}{a_{\text{ema}}[u]}, m, D\right)
        if SP_IN then
 6
             s \leftarrow |W[:,u]|
 7
        else
 8
         s \leftarrow |W[u,:]|
 9
10
         idx \leftarrow TopK(s, k)
                                                                    ▶ Regrowth: Top-k from full row/column
        if SP_IN then
11
              M[:,u] \leftarrow 0; M[idx,u] \leftarrow 1
12
13
             M[u,:] \leftarrow 0; M[u,idx] \leftarrow 1
15 return M
```

bounded, this reduces to $I(Z;Y) \leq \frac{C}{2\sigma^2} \sum_i a_i k_i$, so total traffic serves as a simple proxy for downstream information flow.(derivation in Appendix).

$$I(Z;Y) \le \frac{C}{2\sigma^2} \sum_{i} a_i k_i$$

This indicates that the total traffic in a learning network serves as a tractable upper bound on the downstream information flow. Consequently, a BB refresh that prunes the weakest outgoing edges from high-traffic units produces a descent step on a composite objective $\mathcal{L} = \mathcal{L}_{task} + \lambda \sum_i a_i k_i$ (Lemma in Appendix). Hence, the observed network homeostasis observed in biological networks [1] and in our experiments is a consequences of optimizing a single, principled objective. Specifically, we show that neurons in a budgeted network are more decorrelated than neurons trained with standard methods, while maintaining accuracy, and that total traffic is a good linear predictor of the estimated mutual information.

Input versus output pruning. We also find that the two BB pruning actuators, SP-in and SP-out, provide complementary forces that drive the network toward this balance. A local linear-response analysis (see Appendix) shows that SP-in shocks primarily adjust a unit's activity (a_i) , while SP-out shocks primarily adjust its audience (k_i) . Together, the system can efficiently corrects deviations from the optimal state.

5 Experiments

We first provide clean-room validation of BB's core properties on controlled didactic tasks (balance, safety for rare features, and overcoming optimization barriers), then demonstrate the principle's breadth on large-scale benchmarks (ASR, face identification, change detection), and conclude with a capstone test in synapse segmentation that exercises the method in a 3D U-Net for biomedical imaging.

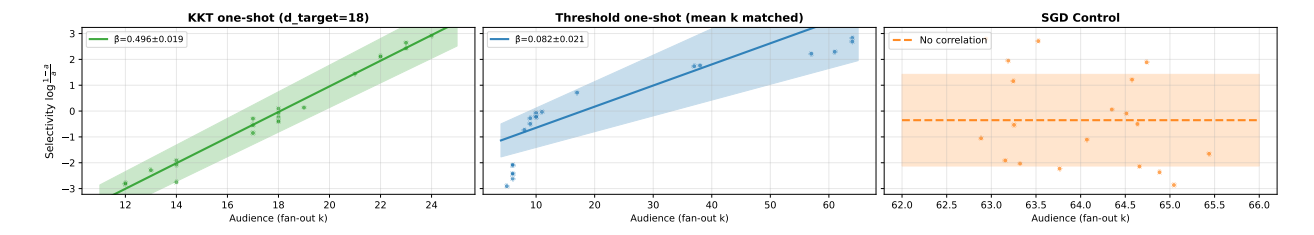


Figure 3: **The selectivity-audience balance emerges under budget pressure on controlled XOR tasks.** The balance is a direct consequence of budget-driven structural adaptation, not an artifact of gradient-based training. **Left panel:** In networks trained with Budgeted Broadcast, a robust linear relationship emerges between unit fan-out (k_i) and inactivity log-odds, confirming our theoretical prediction. **Middle panel:** A one-shot traffic-threshold variant that prunes when $t_i = a_i k_i > \tau$ produces a similar trend but with a wider variability band and mild curvature, consistent with the threshold gate being a local approximation to the KKT stationary law $\log \frac{1-a_i}{a_i} = \beta k_i$. **Right panel:** In control networks trained with SGD alone, fan-out remains constant at the initialization value (64), eliminating any correlation with activity (see Sec. 5.1.1)

5.1 Didactic validation: mechanism, safety, and hardness

We first use simple MLP architectures to investigate three consequences of BB on controlled tasks—mechanism (XOR balance), feature safety (DNF+rare), and optimization hardness (DNF witness). While the specific controller implementation can vary (e.g., using a global budget with adaptive β or a fixed local threshold τ), all variants operate on the same core idea: pruning is triggered when a unit's traffic $t_i = a_i k_i$ becomes excessive. This allows us to cleanly study the emergence of the predicted balance, the inherent safety for rare features, and the ability to overcome optimization challenges.

5.1.1 Emergence of the Selectivity-Audience Balance

To provide a visualization of the selectivity-audience balance, we use a simple 3-layer MLP trained on the XOR task (Input \rightarrow H1(64) \rightarrow H2(128) \rightarrow Output, with ReLU activations). We use SP-out on W_2 (row-mask on W_2) to control the output fan-out of the first hidden layer (H1). Activity (a_i) is measured as the post-ReLU EMA of the H1 units. As shown in Figure 3, this setup produces a stable linear relationship between fan-out (k_i) and the log-odds of inactivity ($\log \frac{1-a_i}{a_i}$), ensuring that the BB mechanism achieves the theoretically predicted balance (100% accuracy; linear fit with slope $\hat{\beta} = 0.5 \pm 0.02$ and $R^2 = 0.98 \pm 0.005$ on non-saturated units across 7 seeds).

5.1.2 DNF Tasks: Safety and Optimization

We study two aspects of BB on Disjunctive Normal Form (DNF; an OR of several AND clauses) tasks: rare-feature safety and optimization barrier removal.

Safety for Rare Features. We first test if the BB rule is able to protect rare but important signals. We construct a DNF task containing features with varying frequencies of activation: rare ($p\approx0.11$), common ($p\approx0.72$), and moderately selective ($p\approx0.22$). As shown in Figure 4a, the BB controller demonstrates remarkable selectivity. The rare feature's traffic ($t_s=a_sk_s$) is low and only moderately reduced to go below the pruning threshold τ . In contrast, the common feature is actively managed, its traffic sharply curbed by pruning. This empirically validates that by budgeting traffic, BB can distinguish between features based on their usage patterns, safeguarding the pathways for infrequent events.

Overcoming an Optimization Barrier. To test BB's ability to reshape learning dynamics, we designed a DNF task that is difficult for standard gradient-based methods. The task uses W + 1 disjoint clauses, where each

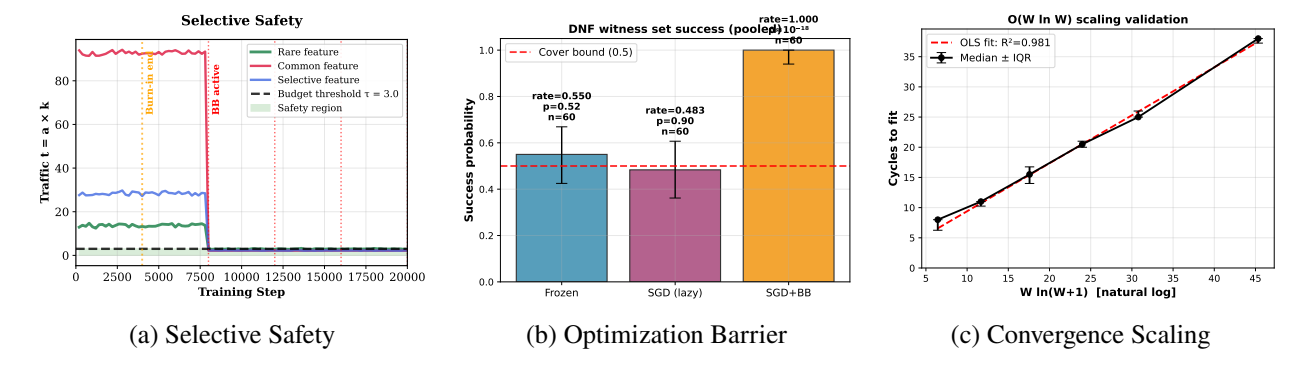


Figure 4: **BB's core properties validated on controlled DNF tasks.** These experiments confirm the mechanism, safety, and optimization benefits of the BB principle. (a) BB inherently protects rare features (green line), whose traffic remains safely below the budget τ , while actively pruning over-active common features (red line). (b) BB consistently solves a DNF task designed to make standard SGD fail, overcoming a lazy-learning barrier. (c) The number of cycles for BB to solve the DNF task follows a predictable $O(W \log W)$ scaling law. All setup details are in Appendix.

AND clause operates on a unique set of inputs. The ideal network should learn a sparse "one-unit-per-clause" representation, allocating one hidden unit for each clause.

This setup creates a severe credit assignment problem for standard SGD, particularly in "lazy" learning regimes where weights change little from their random initialization. We train the network on a witness set, where each input is designed to activate only one specific clause. We predict that when a mini-batch contains witnesses for different clauses, the averaged gradient is weak and ambiguous, failing to specialize any single unit to its target clause, causing the network to get stuck (being unable to break the initial symmetry of its random weights). Theory predicts (and our experiments confirm) that such a learner will fail to solve the problem about half the time (Fig. 4b),consistent with Cover's separability fraction (formalized in Appendix).

In contrast, alternating SGD with our BB controller consistently escapes this barrier. After a few SGD steps, units that responded non-specifically to multiple inputs develop slightly higher average activity. The BB controller, being agnostic to the ambiguous gradients, simply identifies these "uselessly busy" units by their high traffic and prunes their connections. This structural change breaks the learning symmetry, allowing other units to specialize and "capture" a clause in the next training phase. This iterative process acts as a powerful search mechanism. As shown in Figure 4b and 4c, BB consistently solves the task, and the number of cycles required scales predictably as $O(W \log W)$. This empirically matches the "coupon collector" behavior we formally analyze in the appendix), where the network "collects" the solution for each of the W clauses one by one.

Homeostatic Resilience to Structural Shocks. Finally, we tested the dynamic resilience conferred by the BB rule. In a "shock–recovery" experiment, we subjected a trained network to sudden, large-scale pruning events and observed its response. The network exhibited graceful degradation in performance, followed by rapid, autonomous recovery once training resumed. This demonstrates that BB creates not just a statically efficient architecture, but a dynamically stable one with robust homeostatic properties. The full protocol and results are detailed in Appendix.

5.2 Domain 1: Automatic Speech Recognition

To test BB on a foundational sequence-to-sequence task, we employed a standard encoder-decoder Transformer trained on the LibriSpeech ([16]) train-clean-100 dataset. For a controlled comparison, all methods

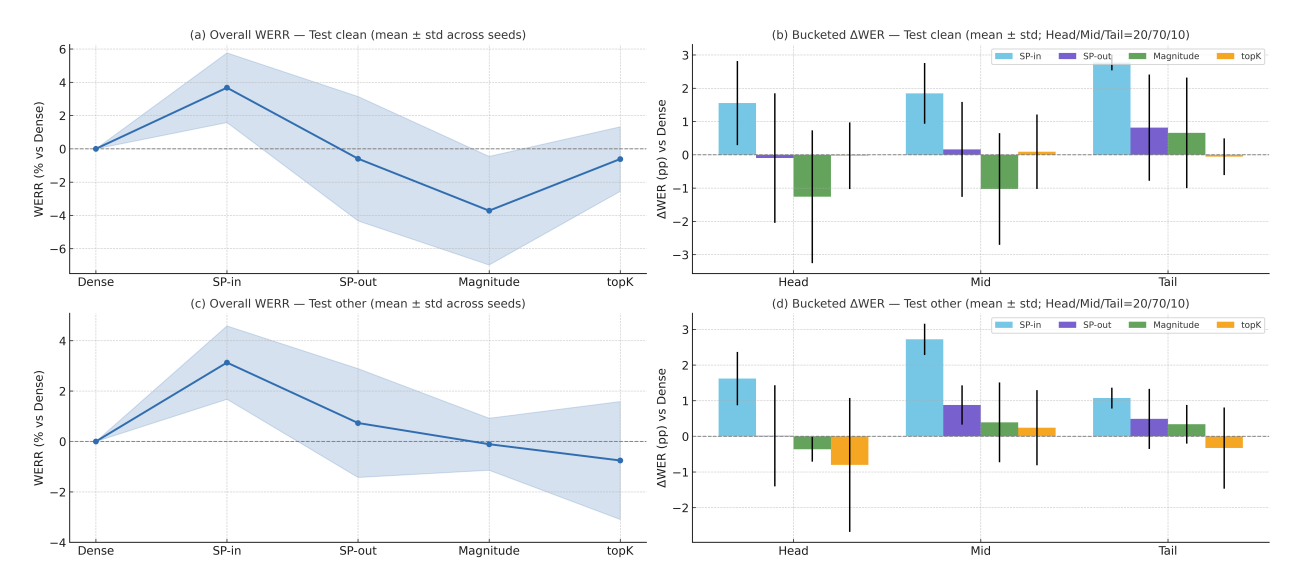


Figure 5: **ASR on LibriSpeech.** (a) Overall Word Error Rate Reduction (WERR) test_clean; (b) Bucketed Δ Word Error Rate (WER) test_clean (Head/Mid/Tail fixed at 20/70/10; buckets are fixed across methods); (c) Overall WERR test_other; (d) Bucketed Δ WER test_other. Shaded bands/bars are mean \pm std over seeds; dashed line is Dense (WERR / Δ WER = 0).

(including baselines) followed an identical three-stage training schedule, beginning with decoder dense pre-training and encoder-only align training before enabling sparsification for the final full-transformer training.

To establish a fair and empirically-grounded sparsity budget, we applied the final network density of 0.85 for all baseline methods, and mask refreshes occurred every 25 optimizer steps with no regrowth rule (detail in Appendix). This setup allowed us to fairly evaluate the impact of different pruning principles on Word Error Rate (WER), particularly on rare words.

Under the identical schedule and budget, BB (SP-in) is consistently best (Fig. 5a,c), while BB (SP-out) is roughly neutral and Magnitude/Top-*k* trails.

To localize gains, Fig. 5b,d report *bucketed* ΔWER using the fixed Head/Mid/Tail buckets. We assign utterances to Head/Mid/Tail by sorting items by frequency and taking disjoint quantiles (20%/70%/10%); buckets are fixed across methods and runs. All results are under matched budget, placement, schedule, and seeds. Averaged across seeds, SP-in improves all buckets and is largest on the long tail; SP-out shows smaller gains; Magnitude is negative on Head and near zero on Mid/Tail. This suggests that while magnitude pruning may harm performance on common words, BB's traffic-based approach reallocates resources to benefit the entire frequency spectrum, especially the challenging long tail.

5.3 Domain 2: Face Identification

For face identification, we utilized a standard ResNet-101 ([17]) backbone with its final layer adapted for the 7,001 identities in our curated VGGFace2-7k dataset [18]. To test BB in a modern convolutional architecture, we applied it as a fan-in mask (SP-in) to the 1×1 projection kernels within each bottleneck block. This specific placement allows us to investigate the effect of budgeting traffic between channels in a ResNet. All sparse methods, including baselines like Magnitude pruning and RigL [19], were applied to the same set of kernels to ensure a fair comparison based on Top-1 classification and verification accuracy.

We pre-specify the budgets before training. Concretely, we sweep six target sparsity levels $s \in \{0.9, 0.7, 0.6, 0.5, 0.4, 0.3\}$ and enforce the same target for all methods on the identical layer subset and fan-in

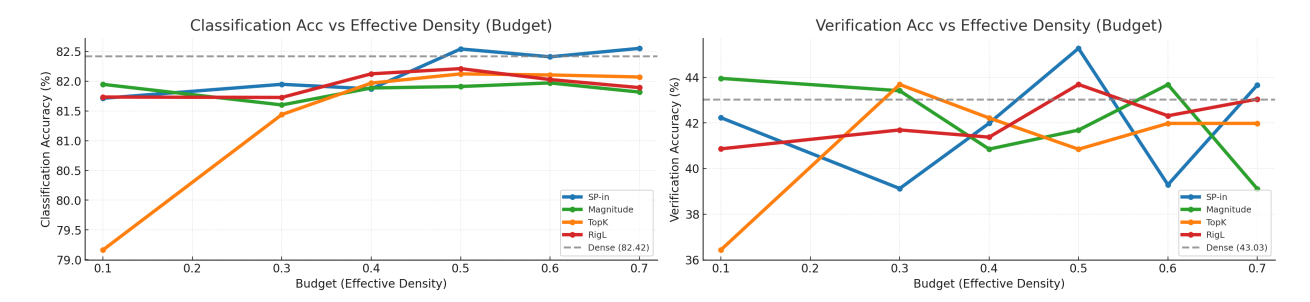


Figure 6: **Pareto fronts on VGGFace2–7k.** *Left*: Top-1 classification accuracy vs. budget (effective density). *Right*: verification accuracy vs. budget on a held-out pair set. Each curve shows the best checkpoint per method at each density; the dense reference is the gray point at 1.0. Across a broad range of budgets, SP-in forms or matches the upper envelope while using fewer active parameters



Figure 7: Change detection on LEVIR-CD: Dense vs. SP-in (top-k qualitative). Top: A (t1), B (t2), and Ground Truth. Bottom: *Dense-only* TPs within GT (red), *SP-in-only* TPs within GT (green) Shown is the test image with the highest Δ TP.

masking side. Masks are refreshed every 200 optimizer steps with regrowth enabled at each refresh (i.e., previously pruned edges may re-enter via top-k). This protocol isolates the pruning principle itself under matched budgets and placement (details in Appendix).

For each density, we sweep 30 epochs and pick the best validation checkpoint per method. Fig. 6 plots *Top-1* (left) and *verification* (right) against effective density. Across 0.3–0.7, SP-in forms or matches the upper envelope and often exceeds the dense references around 0.5–0.7. RigL is competitive at higher densities; magnitude degrades as sparsity increases; activation Top-*k* shows inconsistent peaks but does not dominate.

5.4 Domain 3: Change Detection

To evaluate BB's performance in a pixel-wise prediction task, we addressed bi-temporal building change detection on the LEVIR-CD dataset [20]. We used a lightweight, Siamese encoder-decoder architecture (FC-Siam-conc) that processes two temporal images to produce a binary change mask. For this model, SP-in was applied as a fan-in mask to the first 3×3 convolution in each encoder block, with the decoder remaining dense. We report mean Intersection-over-Union (IoU) and F1-score on the held-out test set, comparing against the unpruned dense model under an identical training schedule.

We compare BB(SP-in) against the dense model without pre-specifying a sparsity target using default hyperparameters. This yields a final global density of 0.70. Masks use a warm-up of 1,000 optimizer steps, then refresh every 50 steps, with regrowth enabled at each refresh (i.e., previously pruned edges may re-enter via top-k). This protocol ensures a fair comparison under matched placement and schedule while allowing SP-in to discover an empirically grounded budget (details in Appendix).

Under the same 30-epoch schedule and fixed decision threshold, SP-in improves over Dense in all runs, as summarized below.

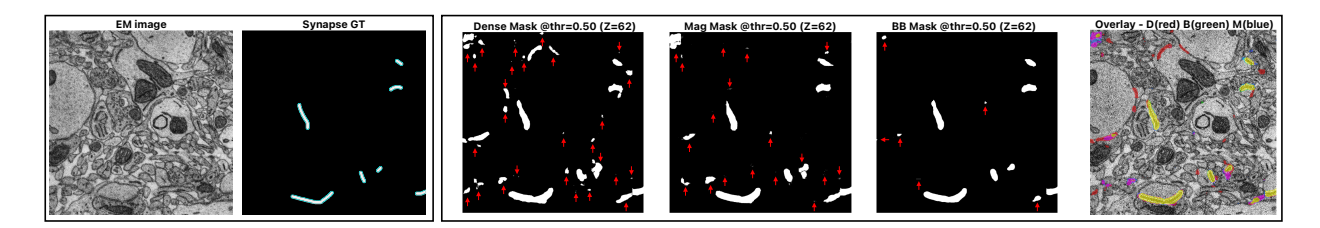


Figure 8: **Synapse prediction (per-method Best-F1).** Qualitative overlays and operating-point comparison. Red arrows denote false negatives (omitted GT synapses). Right overlay: Dense=red, BB=green, Mag=blue; yellow marks consensus. Further details in Appendix.

| Method | PR-AUC | ROC-AUC | BestF1 | BestIoU |
|------------|--------------------|------------------------|---------------------|---------------------|
| Dense | 0.6952 ± 0.010 | 0.9889 ± 0.0004 | 0.6578 ± 0.0070 | 0.4906 ± 0.0080 |
| BB (SP-in) | 0.7407 ± 0.014 | 0.9906 ± 0.0006 | 0.6752 ± 0.0090 | 0.5099 ± 0.0100 |
| Mag | 0.7253 ± 0.019 | 0.9896 ± 0.0009 | 0.6643 ± 0.0120 | 0.4981 ± 0.0140 |

Table 1: **Synapse prediction (3 seeds, mean±std).** Results are computed at each method's own Best-F1 threshold and then averaged across seeds.

Averaged across runs, this represents a relative improvement of **+10.8**% in IoU and **+7.9**% in F1 (details in Appendix).

SP-in recovers substantially more true positives *inside* the GT regions, especially for small, spatially scattered changes, while preserving major detections shared with Dense.

5.5 Domain 4: Synapse Prediction (EM)

As a capstone test of architectural generality, we applied BB(SP-in) (magnitude-based, row-wise fan-in masks) to a residual–SE 3D U-Net for synapse segmentation on volumetric EM from the SmartEM dataset ([21]; GT1 for training, GT2 held-out for testing). Concretely, we attach BB to all main $3 \times 3 \times 3$ convolutions (both conv1 and conv2) across encoder and decoder blocks, while leaving ConvTranspose upsampling layers and skip concatenations dense. We compare against a dense baseline and a standard magnitude pruning baseline, reporting PR-AUC and Best F1 on the held-out test set.

For synapse prediction, we use a fixed budget ratio of 0.70, apply a 1,000-step warm-up, then linearly ramp to the target over 8,000 steps; masks are refreshed every 200 optimizer steps, with variance-preserving rescaling $\sqrt{\text{prev/cur}}$ per output channel. Pruning is applied to all Conv3d layers in encoder and decoder blocks (including SE 1×1×1 and residual 1×1×1 projections), while ConvTranspose3d upsampling layers and skip concatenations remain dense. Dense and pruned models share the exact same pipeline; inference uses sliding windows with 8× flip TTA, and we report PR-AUC and best F1 on the held-out GT2 set ((detail in Appendix)).

6 Discussion & Future Work

This work introduces a new axis for structural plasticity in artificial neural networks, shifting the focus from a component's *utility* to its metabolic *cost*. We formalized this cost as traffic $(a_i k_i)$ and showed that a simple, local budget on this traffic can organize connectivity. The emergent selectivity-audience balance $(\log \frac{1-a_i}{a_i} \approx \beta k_i)$ is a predictable equilibrium that links structure (k_i) to function (a_i) . This computational framework provides a unified explanation for seemingly distinct biological phenomena from Henneman's size

principle [4] to the competitive dynamics of synapse elimination [1], reframing them as convergent solutions to the universal problem of efficient information broadcast. The success of our Budgeted Broadcast rule on diverse benchmarks provides empirical support for this structural perspective of neural organization.

Future work should study application of budgeted neural activity beyond FFNs and CNNs, and in particular to lateral connections and attention models. While our method introduces modest, amortized overhead from EMA tracking and periodic mask updates, its scalability makes it a promising candidate for foundation models where protecting the long tail of knowledge is paramount.

A Budgeted Attention mechanism would extend our per-neuron budget to a dynamic, per-token budget. A token's 'traffic' could be defined as $t_j = f(A_j) \times k_{\text{eff}}(j)$, where $f(A_j)$ is a function of the token's activation norm (how 'loud' it is) and $k_{\text{eff}}(j)$ is its *effective fan-out*.

References

- [1] Barber, Mark J. and Lichtman, Jeff W.; Activity-Driven Synapse Elimination Leads Paradoxically to Domination by the Remaining, Less Active Axon; Journal of Neuroscience; 1999.
- [2] Hengyuan Hu and Rui Peng and Yu-Wing Tai and Chi-Keung Tang; Network Trimming: A Data-Driven Neuron Pruning Approach Towards Efficient Deep Architectures; arXiv preprint arXiv:1607.03250; 2016.
- [3] Amari, S-I; Information geometry on hierarchy of probability distributions; IEEE transactions on information theory; 2002.
- [4] Henneman, Elwood; Relation between size of neurons and their susceptibility to discharge; Science; 1957.
- [5] Henneman, E. and Somjen, G. and Carpenter, D. O.; Functional significance of cell size in spinal motoneurons; Journal of Neurophysiology; 1965.
- [6] Han, Song and Pool, Jeff and Tran, John and Dally, William; Learning both weights and connections for efficient neural network; Advances in Neural Information Processing Systems; 2015.
- [7] Han, Song and Mao, Huizi and Dally, William J.; Deep Compression: Compressing Deep Neural Networks with Pruning, Trained Quantization and Huffman Coding; International Conference on Learning Representations; 2016.
- [8] Gordon, Ariel and Eban, Elad and Nachum, Ofir and Chen, Bo and Wu, Hao and Yang, Tien-Ju and Choi, Edward; MorphNet: Fast & Simple Resource-Constrained Structure Learning of Deep Networks; Proceedings of the IEEE/CVF Conference on Computer Vision and Pattern Recognition; 2018.
- [9] LeCun, Yann and Denker, John S and Solla, Sara A; Optimal brain damage; Advances in Neural Information Processing Systems; 1990.
- [10] Frankle, Jonathan and Carbin, Michael; The Lottery Ticket Hypothesis: Finding Sparse, Trainable Neural Networks; International Conference on Learning Representations; 2019.
- [11] Tanaka, Hidenori and Kunin, Daniel and Yamins, Daniel and Ganguli, Surya; Pruning Neural Networks without any Data by Iteratively Conserving Synaptic Flow; Advances in Neural Information Processing Systems; 2020.

- [12] Dasgupta, Sanjoy and Meirovitch, Yaron and Zheng, Xin and Bush, Ian and Lichtman, Jeff W. and Navlakha, Saket; A neural algorithm for computing bipartite matchings; Proceedings of the National Academy of Sciences; 2024.
- [13] Turrigiano, G. G. and Nelson, S. B.; Homeostatic plasticity in the developing nervous system; Nature Reviews Neuroscience; 2004.
- [14] Lee, Namhoon and Ajanthan, Thalaiyasingam and Torr, Philip H. S.; SNIP: Single-shot Network Pruning based on Connection Sensitivity; International Conference on Learning Representations; 2019.
- [15] Wang, Chaoqi and Zhang, Guodong and Grosse, Roger; Picking Winning Tickets Before Training by Preserving Gradient Flow; International Conference on Learning Representations; 2020.
- [16] Panayotov, Vassil and Chen, Guoguo and Povey, Daniel and Khudanpur, Sanjeev; Panayotov2015LibriSpeech; ICASSP; 2015.
- [17] He, Kaiming and Zhang, Xiangyu and Ren, Shaoqing and Sun, Jian; Deep Residual Learning for Image Recognition; Proceedings of the IEEE Conference on Computer Vision and Pattern Recognition; 2016.
- [18] Cao, Qiong and Shen, Li and Xie, Weidi and Parkhi, Omkar M. and Zisserman, Andrew; VGGFace2: A Dataset for Recognising Faces across Pose and Age; 2018 13th IEEE International Conference on Automatic Face & Gesture Recognition (FG 2018); 2018.
- [19] Evci, Utku and Gale, Trevor and Menick, Jacob and Castro, Pablo Samuel and Elsen, Erich; Rigging the Lottery: Making All Tickets Winners; Proceedings of the 37th International Conference on Machine Learning; 2020.
- [20] Chen, Hao and Shi, Zhenwei; A Spatial-Temporal Attention-Based Method and a New Dataset for Remote Sensing Image Change Detection; Remote Sensing; 2020.
- [21] Meirovitch, Yaron and Park, Core Francisco and Mi, Lu and Potocek, Pavel and Sawmya, Shashata and Li, Yicong and Wu, Yuelong and Schalek, Richard and Pfister, Hanspeter and Schoenmakers, Remco and others; SmartEM: machine-learning guided electron microscopy; bioRxiv; 2023.

APPENDIX for Budgeted Broadcast: An Activity-Dependent Pruning Rule for Neural Network Efficiency

Will be released with the published paper.